

Sediment shell-content diminishes current-driven sand ripple development and migration

Chiu H. Cheng^{1,2}, Jaco C. de Smit^{1,3}, Greg S. Fivash¹, Suzanne J. M. H. Hulscher⁴, Bas W. Borsje⁴, Karline Soetaert¹

5 ¹NIOZ Royal Netherlands Institute for Sea Research, Department of Estuarine and Delta Systems (EDS), 4400 AC Yerseke, The Netherlands.

²Wageningen Marine Research, Wageningen University & Research, 4400 AB Yerseke, The Netherlands.

³Faculty of Geosciences, Department of Physical Geography, Utrecht University, 3584 CB Utrecht, The Netherlands.

⁴Water Engineering and Management, University of Twente, 7500 AE Enschede, The Netherlands.

10

Correspondence to: Chiu H. Cheng (chiu.cheng@nioz.nl)

15

20

25 **Abstract.** Shells and shell fragments are biogenic structures that are widespread throughout natural sandy shelf seas and whose
presence can affect the bed roughness and erodibility of the seabed. An important and direct consequence is the effect on the
formation and movement of small bedforms such as sand ripples. We experimentally measured ripple formation and migration
of a mixture of natural sand with increasing volumes of shell material in a racetrack flume. Our experiments reveal the impacts
of shells on ripple development in sandy sediment, providing information that was previously lacking. Shells expedite the
30 onset of sediment transport while simultaneously reducing ripple dimensions and slowing down their migration rates.
Moreover, increasing shell content enhances near-bed flow velocity due to the reduction of bed friction that is partly caused
by a decrease in average ripple size and occurrence. This, in essence, limits the rate and magnitude of bedload transport. Given
the large influence of shell content on sediment dynamics on the one hand, and the high shell concentrations found naturally
in the sediments of shallow seas on the other hand, a significant control from shells on the morphodynamics of sandy marine
35 habitats is expected.

40

45

50

55

1 Introduction

Ripples are the most common bedforms found in the marine environment, including in shallow, sandy environments (Bartholdy et al., 2015; Langlois and Valance, 2007). They form over a broad range of sandy grain mixtures under low energy flow or wave conditions that exceed the erosion threshold (Precht and Huettel, 2003; Soulsby, 1997). With increasing water depth, ripples become progressively driven by currents rather than waves. Current-generated ripples are very dynamic microscale bedforms, with typical sizes of around 0.1 m in wavelength and up to 0.01 m or more in height (Ashley et al., 1990; van Rijn et al., 1993). They continuously develop and erode, typically on the order of minutes to days, and can migrate at rates exceeding 0.4 cm min⁻¹ (Baas et al., 2000; Baas and De Koning, 1995; Bartholdy et al., 2015; Lichtman et al., 2018). As the ripples move and change in dimension, the bed roughness is correspondingly altered, which can have cascading effects on the surrounding areas such as larger bedforms (e.g., tidal sand waves) on which they are often superimposed (Brakenhoff et al., 2020; Damveld et al., 2018, 2019; Idier et al., 2004). Additionally, ripples also generate distinct spatial variations in sediment composition and alter the distribution of particulate organic matter by their effect on hydrodynamics, some of which can further modify the sediment properties in ways that influence erosion (Ahmerkamp et al., 2015; Kösters and Winter, 2014; Mietta et al., 2009).

Shells, a biogenic material created by marine bivalves, are widely distributed in certain regions of the marine environment (Russell-Hunter, 1983). These calcareous structures remain present long after the death of the organisms (Gutiérrez et al., 2003; Kidwell, 1985), and they are mostly found in the form of separated single shell valves and shell fragments. In environments where shells are prevalent, they may constitute 20–70 % of the total sediment composition (by volumetric percentage), although even higher percentages have been observed in very extreme cases (Dey, 2003; Soulsby, 1997). Since they have a lower bulk density, their presence reduces the bulk density of the sediment by diluting the quartz fraction (Soulsby, 1997). As shell material is rather plate-like, irregular and angular in shape, they also change the general composition compared to the smaller, surrounding sediment particles (Al-Dabbas and McManus, 1987). Intact shells and larger fragments may inhibit sediment transport through bed armoring. Armoring occurs when the mean shear stress is below the critical erosion threshold for the coarsest fractions, but above that for the finer particles, resulting in their entrainment. This winnowing causes the surface to become coarser and coarser, essentially building up an armor layer (Vericat et al., 2006). In riverine environments, coarse material such as gravel has been shown to facilitate bed armoring, causing the upper layers of the sediment to become significantly coarser than the median grain size (D_{50}) of the sediment beneath, ultimately reducing or inhibiting sediment transport (Curran, 2010; Wilcock and Detemple, 2005). Shells may also be able to provide a similar armoring effect against sand erosion given that they are more difficult to erode (Miedema and Ramsdell, 2011; Ramsdell and Miedema, 2010).

Thus far, very few studies have investigated the direct influence of shell material on the bedload transport dynamics through the alteration of bed roughness (Gutiérrez et al., 2003; Nowell and Jumars, 1984). Some studies have explored the ways in which shells could be used as tracers for sediment motion, given their widespread occurrence (Al-Dabbas and McManus, 1987). The drag and incipient motion of the valves of a few bivalve species have also been investigated in the

laboratory (Dey, 2003). Similar studies have focused on the erosion and settling velocities of shells, based on shapes, shell positioning and associated drag, being transported through a pipeline (Miedema and Ramsdell, 2011; Ramsdell and Miedema, 2010). Although these studies have considered how the irregularity in shape and orientation of shell valves potentially interact with flow, the focus has been more within a hydrodynamic context rather than a sedimentary one. To our knowledge, there have not been studies addressing the direct effects of a natural, representative mixture of shells and sandy sediment on the development and movement of ripples.

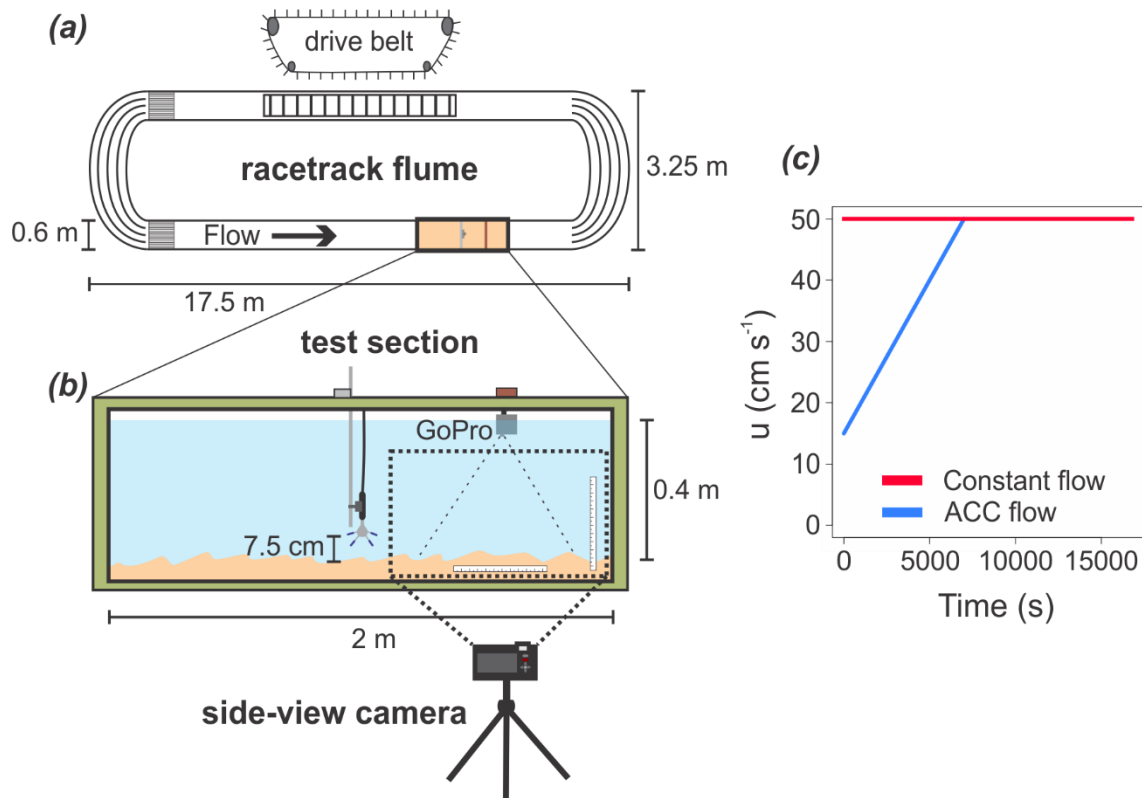
From a hydraulic point of view, biogenic materials such as shells do not exhibit the same response as compared to rock fragments of a similar size, although some shells (e.g., the mussel family, Mytilidae) have been shown to behave more similarly to the smaller sand particles (Al-Dabbas and McManus, 1987). However, due to the shape and size of most shells, combined with their lower density, they are known to have a much lower settling velocity and much larger erosion velocity threshold than sand particles (Ramsdell and Miedema, 2010). The mere presence of empty shells has also been shown to facilitate silt and other fine-particle entrainment in the sediment (Huettel and Rusch, 2000; Pilditch et al., 1997; Witbaard et al., 2016). But despite their prevalent nature and potential to affect sediment dynamics in several ways, there is at present a knowledge gap in terms of the direct influence of shells on the geomorphology of sandy sediments.

The objective of this experiment was to determine the effect of biogenic shells on the development of ripples in medium sand, in relation to unidirectional flow and turbulence along the bed. The combination of flow velocity and turbulence intensity largely dictates the sediment dynamics, thereby affecting bedform development and sediment stability (Blanchard et al., 1997; Herman et al., 2001; Paterson et al., 2001). Bottom roughness and small-scale topography are important contributing factors to bedform pattern development (Van Oyen et al., 2010), and past studies have found a significant effect of epibenthic structures at different densities (e.g., mimics of tube worm reef patches) on flow and sediment erosion (Friedrichs et al., 2000, 2009). However, the influence of shell material on the ripple dynamics, in relation to flow and turbulence, is still not well understood. Thus, we aimed to quantify the turbulence generated by the flow along sand ripples, simulating scenarios both with and without the presence of shells. We used shells from common bivalve species found in the sandy Dutch North Sea including *Spisula* spp., *Tellimya* spp. and *Cerastoderma edule*, at increasing densities. Using empty shells, we determined the influence, via autogenic engineering, of shell material on sediment transport by testing the effects of increasing shell content on ripple formation, shape and migration rates.

Our paper is organized as follows. The experimental setup, instrumentation and analyses utilized are described in section 2. The results, including the incipient sediment motion, ripple migration and other ripple calculations are presented in section 3. The significance of our findings are discussed in section 4. In section 5, the final conclusions are presented.

2.1 The experimental setup

Our experiments were performed in a racetrack flume facility located at the NIOZ Royal Netherlands Institute for Sea Research, Yerseke, The Netherlands. This large, unidirectional flow channel measures approximately 17.5 m in length and 3.25 m in width and can generate depth-averaged currents up to 60 cm s^{-1} (Fig. 1a). A test section containing a sediment basin measuring $200 \times 60 \times 25 \text{ cm}$ (L x W x H) is located at the far end of one of the long, straight sections of the flume to minimize the effect of bend flows (Fig. 1b). The drive belt equipped on the backside allows the flow to be controlled with high precision.



130 **Figure 1:** (a) The top view of the NIOZ racetrack flume. (b) A side view of the 2 m long test section showing the ADV vectrino, GoPro and side-view cameras used in each experimental run. Both cameras were positioned within the 2nd half of the viewing window of the test section. (c) The flume flow settings implemented in the two separate experiments. *Note:* Although ripples are shown for illustrative purposes, the indicated water depth and ADV height are based on the initial (flat bed) condition.

The basin of the 2 m test section was filled using North Sea sandy sediment (see Table S1 for the properties). To maintain a sediment supply throughout the duration of each individual experiment, a thin layer of sand ($\sim 3 \text{ cm}$) was also placed

135 over the 3 m preceding the measurement section of the flume track. The bed was fully mixed and flattened before each experimental run. The total water depth was 40 cm and only freshwater was used.

For the shell treatments, we used a mixture that consisted of, on average, approximately 29 % intact shells valves and 71 % fragments (in absolute number of pieces). All non-shell materials (e.g., rocks and wood detritus) were removed prior to the addition. We took a random sampling of the shell stockpile to determine the average dimensional properties of the shell valves and fragments (Table S2; Fig. S1).
140

Two separate experiments were conducted. A constant flow experiment was used to measure equilibrium ripple dimensions and migration rates. An acceleration (ACC) flow experiment was run to measure the incipient sediment motion. The flow settings used in the two experiments are shown in Fig. 1c. Both experiments consisted of several experimental runs, which were varied by changing the volumetric percentage of shell content. The control (0 % shells) contained only sandy sediment, while each subsequent treatment was modified by the addition of shell material. The volumetric percentage of shell increased by 2.5 or 5 % intervals, up to 30 %, while the last two treatments contained 40 % and 50 % shells, respectively. The flume was filled with water overnight, and all experimental runs were always performed the very next day to maintain consistency (e.g., minimize variability due to compaction, etc.). The constant flow experiment consisted of six treatments (0, 5, 10, 15, 20, and 50 % shell), while the ACC flow experiment included 11 treatments (0, 2.5, 7.5, 10, 12.5, 15, 20, 25, 30, 40 and 50; see Table S3 for a summary of the experimental settings and measurements).
145
150

2.2 Constant flow experiment

In the constant flow experimental runs, a 50 cm s⁻¹ depth-averaged flow velocity was maintained for more than 4 hours, so as to achieve equilibrium conditions (Fig. 1c). Preliminary runs showed that morphological equilibrium was achieved well within one hour at this flow rate. A Canon EOS 1000D camera, equipped with an EX Sigma lens (DG Macro, 50 mm, 1:2.8) was positioned at the side of the flume, targeting the 2nd half of the test section to record time-lapse photos from the side at 10-second intervals. The photos recorded a section 76.5 cm in width and 51 cm in height. Two rulers were attached at the edges of the frame as dimensional guides for the image analyses (Fig. 1b).
155

Concurrently, a Nortek Vectrino ADV profiler was used to record the 3-dimensional flow rates, through coherent Doppler processing, at a frequency of 30 Hz. Data was filtered for minimum correlation values of 90 %, minimum signal-to-noise ratio of 20 dB and minimum amplitude of -35 dB. The probe was placed approximately 7.5 cm above the bed, which was initially flat in each experimental run. With a blanking distance of 4 cm, it measured the bottom section of the water column from 0 to 3.5 cm above the initial flat bed, over a total of 35 cells (1 mm intervals). The ADV was held in place through the duration of the experimental run. Therefore, near-bed flow profiles were corrected for changing bed elevation during ripple migration.
160

165 2.3 Sediment image processing

Identification of ripples within the sediment bed was performed through image analysis of the photo time-series obtained by the camera. The vertical position of the sediment-water interface was identified using Canny edge detection of the green band with the *wvtool* R package (Sugiyama and Kobayashi, 2016), which showed highest contrast. Gamma transformation of the green band further enhanced this contrast to improve the quality of the detection. The fine-grain noise in the sediment surface was filtered out using a low-pass 2nd-order Butterworth filter to produce a smooth surface from which peaks and troughs can be easily identified, using the *signal* R package (Ligges et al., 2015). Ripples were then classified from the identified sediment surface using peak analysis, which isolated peaks and troughs in the sediment surface with the *pracma* R package (Borchers, 2019). This ultimately allowed us to characterize the dimensions of individual ripples and track their movement and development in time. Using 1600 unique frames from each of the six constant flow experimental runs, we quantified the following ripple parameters: (1) the ripple height, (2) length, (3) asymmetry and (4) migration rate.

Each ripple was defined as encompassing the region between two neighboring troughs, separated by a peak. The ripple height and length were defined as the maximum vertical and lateral extent of the ripple. The ripple asymmetry was defined as the difference in length between the two halves of the ripple, separated by the center of its peak, divided by its total length (trough-trough); values change from 0 (highest symmetry) to 1 (highest asymmetry). The migration rate was calculated as the total distance travelled by the peak of a unique ripple over 24 frames (constituting an interval of four minutes). This frame interval allowed ripples to travel measurable distances while limiting the likelihood of them moving out of frame before measurements could be taken. All four of the ripple parameters were measured throughout the experimental duration using each frame. Only whole ripples were used in the analyses, as ripples that were partially in (upstream) or out (downstream) of the frame were excluded. Given that the migration rate was calculated over 24 frames, measurements were not generated from the first or last 23 frames in each run. All image analyses were conducted in R version 3.4.4 (R Core Development Team 2020).

2.4 Near-bed flow calculations

The near-bed turbulent kinetic energy (TKE) was derived from the near-bed flow velocity fluctuations (Pope et al., 2006). This value indicates the mean kinetic energy associated with eddies from the turbulent flow. It is a more-robust method for determining the bed shear stress than e.g., quadrant analysis or Reynold's stress, as these are highly sensitive to the orientation of the ADV profiler. The near-bed TKE was calculated from near-bed flow velocity fluctuations in the x, y and z directions as:

$$TKE = 1/2 \left(\overline{u'_{b,x}{}^2} + \overline{u'_{b,y}{}^2} + \overline{u'_{b,z}{}^2} \right) \quad (1)$$

195

where $\overline{u'_{b,x}}$, $\overline{u'_{b,y}}$ and $\overline{u'_{b,z}}$ represent the root-mean-squares of the near-bed flow velocity fluctuations in the x, y and z directions, respectively. These values were extracted from the flow velocity signal through means of applying a 0.1 Hz high-pass 5th order Butterworth filter. This ensures removal of the background velocity during the measurement period. Another 10 Hz low-pass 5th order Butterworth filter was used to remove the higher frequencies where the signal was dominated by noise.

200 The corresponding bottom shear stress (BSS) was calculated as (Soulsby, 1983):

$$BSS = 0.19\rho TKE \quad (2)$$

Where ρ is the water density (1000 kg m⁻³ for freshwater). Subsequently, the corresponding total bed roughness, which is
205 affected by both shells and bed forms, can be calculated from the depth-averaged velocity and the BSS. For a unidirectional flow, the BSS can be calculated from the depth-averaged velocity as (van Rijn, 1993):

$$BSS = \rho g u^2 / C^2 \quad (3)$$

210 Where u is the depth-averaged velocity (m s⁻¹), g is the gravitational acceleration (9.81 m s⁻²) and C is the Chézy roughness coefficient (m^{0.5} s⁻¹). The Chézy roughness coefficient is a function of the water depth and bed roughness (van Rijn, 1993):

$$C = 18 \log(12h/ks) \quad (4)$$

215 Where h is the water depth (0.4 m in this flume experiment), and ks is the total bed roughness (m) by combined grain friction and form drag.

2.5 ACC flow experiment

This experiment was conducted to measure the onset of incipient sediment transport, as well as the corresponding boundary
220 layer conditions. Incipient sediment transport was measured for a flat bed configuration in order to quantify the direct effect of shells on sediment stability. Sandy sediment with a D_{50} of 350 μm is not expected to exhibit sediment motion below about 30 cm s⁻¹ (van Rijn, 1993), and an initial test run with our setup showed that there was indeed no sediment movement occurring below 20 cm s⁻¹. Thus, the starting velocity of each run was set at 15 cm s⁻¹. The flow speed was linearly increased at a rate of 0.3 cm s⁻¹ per minute from 15 to 50 cm s⁻¹ (over a time frame of 116.6 minutes).

225 The ADV profiler was again anchored in the middle of the test section. One GoPro Hero3 camera was positioned just below the water surface, looking downward, 1.5 m along the test section to produce top-view video recordings of the sediment surface at 2 frames per second. The onset of incipient motion, which was defined as the frequent movement of particles across the entire flume area, was derived visually from the GoPro footage (van Rijn 1993). Visual observation is an accurate method

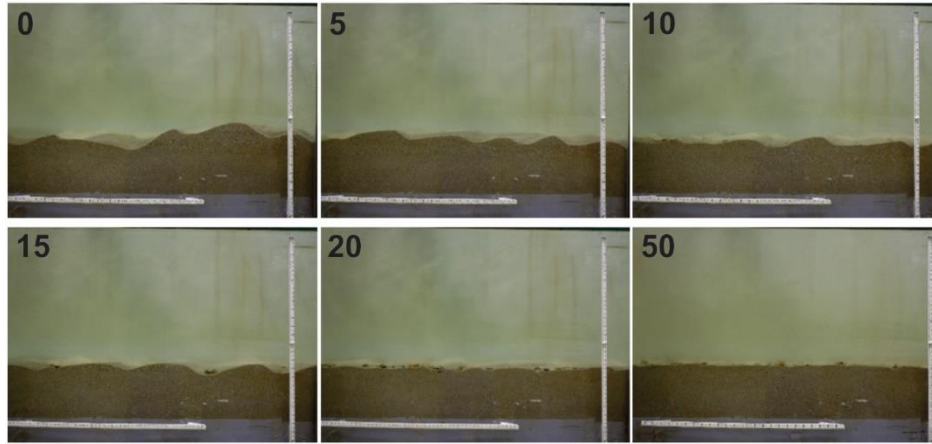
to determine erosion thresholds. As bed load transport is proportional to flow velocity to the power of 3, a small change in velocity will lead to a significant and well-observable change in sediment transport. The depth-averaged velocity was determined from the flume setting at the identified time when incipient motion was observed (Fig. 1c). The critical mean near-bed flow velocity, TKE and BSS were derived from the ADV measurements over the 5 minutes preceding and 5 minutes after the onset of incipient motion following Equations (1) and (2). The total bed roughness for flat beds with varying shell content was calculated following Equations (3) and (4), using a 10-minute window of ADV measurements at an average flow rate of 20 cm s⁻¹, before any ripples had formed.

3 Results

We tested a large range in the shell content in our constant flow experiment, and the results clearly demonstrate that the reduction of ripples is strongly correlated to the shell fraction of sandy sediments. Consequently, the ripple height, length and migration rate were all significantly reduced by the increasing shell content, while the ripple shape became slightly more asymmetric. In the constant flow experiments, the ripples appeared to achieve equilibrium conditions within the first hour at a flow rate of 50 cm s⁻¹. The change in ripple length and height, in particular, can clearly be seen in the concluding frames of each experimental run, particularly around 20 % shell content in the constant flow experiment (Fig. 2a). The ripple height, length, asymmetry and migration rate were not measured in the ACC flow experiment, as we were interested in determining the incipient motion from these runs. Nevertheless, a similar observation could still be seen at around 15 % shell content, even though these ripples were less equilibrated given the lower flow rates for much of the experimental duration (Fig. 2b). In addition, as the shell percentage increased in the experimental runs, they began to exhibit larger, denser aggregations (Fig. 3). What appeared to be bands of shells were actually immobile surficial shells that would periodically appear or disappear as ripples migrated over them. Furthermore, the already-smaller ripples were observed from the GoPro videos to either migrate around the denser and slightly higher positioned shells, or disappear altogether, so the shells did not incorporate themselves into the (migrating) ripples. Even in the lower shell concentrations, where larger ripples frequently migrated over the sparser quantity of shells, the vast majority of these surficial shells were not moved by either the moving ripples or flow (Fig. S2). By performing two types of measurements, we investigated both the (theoretical) equilibrium situation at constant high flow conditions (50 cm s⁻¹), as well as the sequence of events that occur as the velocity increases (the ACC flow experiment). The latter pointed to the physical conditions under which sediment dynamics begin to change (e.g., incipient motion).

255

(a) Constant flow experiment



(b) ACC flow experiment

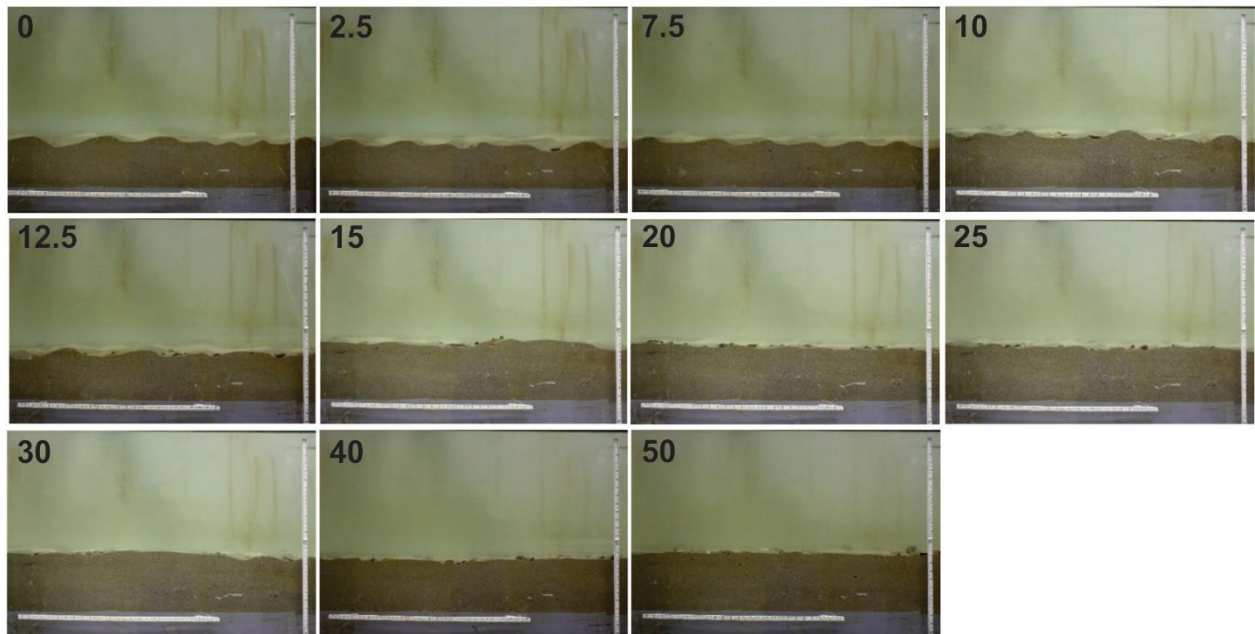
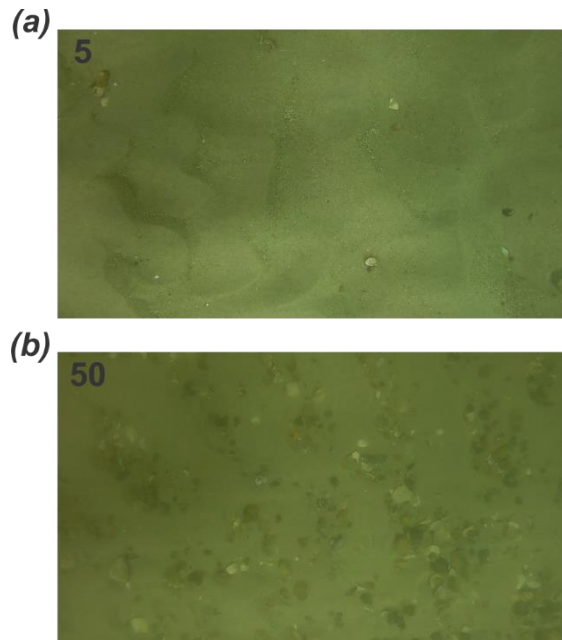


Figure 2: The final frame from each (a) Constant flow and (b) ACC flow experimental run. Numbers represent the shell %. The white vertical and horizontal rulers are both 50 cm in length.

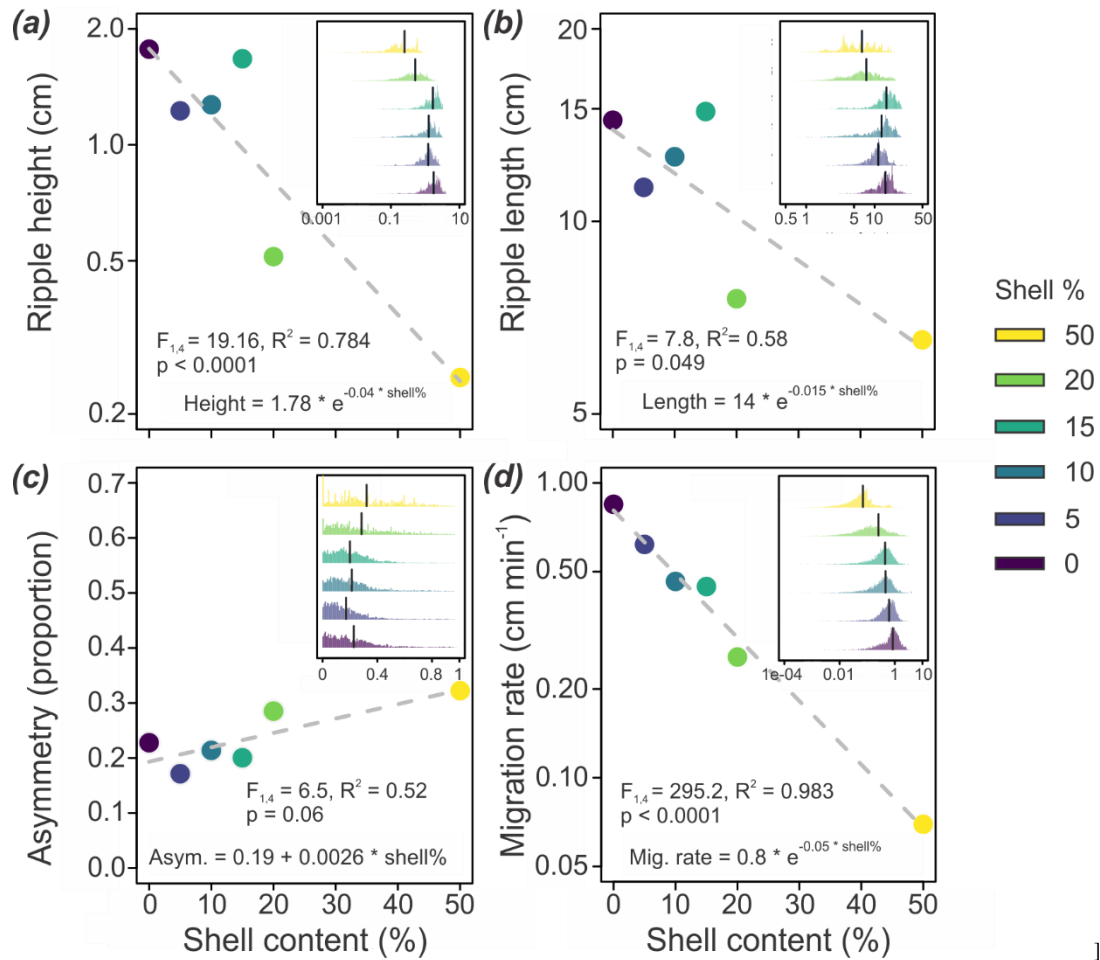


260

Figure 3: Stills taken from the GoPro videos (constant flow experiment) to show the contrast between a (a) low-density and (b) high-density treatment. Shells increasingly appear as immobile clusters at higher concentrations, as they are periodically exposed due to sand movement. The numbers represent the shell %.

3.1 Changes to ripple characteristics (constant flow experiment)

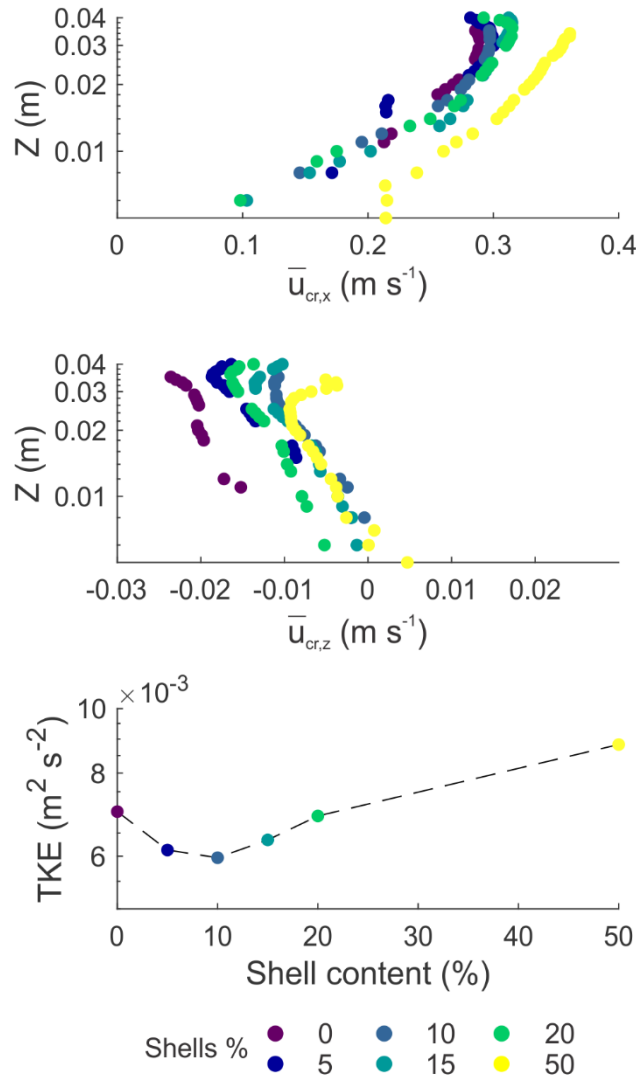
265 An increase in the shell percentage reduced the spatial dimensions of the ripples, and all of the ripple parameters, except ripple symmetry, were highly affected by the presence of shells. The ripple height, length and migration rate all decreased exponentially as a function of shell content, such that the ripples almost entirely disappeared at 50 % shell content (Fig. 2). The ripples also became slightly more asymmetric with increasing shell content (Fig. 4c). Overall, the lengths and heights of the ripples decreased at an average rate of $-0.03 \text{ cm shell } \%^{-1}$ for the height, and $-0.16 \text{ cm shell } \%^{-1}$ for the length (Fig. 4a and
270 b). Ripple asymmetry increased at an average rate of $0.002 \text{ shell } \%^{-1}$ (Fig. 4c). The migration rate showed a consistent decrease with increasing shell content, slowing at an average rate of $-0.016 \text{ cm min}^{-1} \text{ shell } \%^{-1}$ (Fig. 4d). Approximately 18, 20, 14, 13, 13, and 12 ripples were included in the calculations for each experimental run (from 0 to 50 % shell content; Fig. S3).



275 **Figure 4: (a) Ripple height, (b) Ripple length, (c) Asymmetry and (d) Migration rate, plotted against the shell content from the constant flow experimental runs (n = 6). The y-axis of the ripple height, length and migration are plotted under a log scale. Inset panels: The corresponding histograms for each ripple parameter, with the x-axis values representing the y-axis values of the respective regression plots. Vertical lines represent mean values.**

3.2 Changes to near-bed hydrodynamics and critical BSS

280 In the constant flow experiment, the presence of shells (at all percentages) enhanced the near-bed flow in the streamwise direction (Fig. 5a), as ripple sizes become diminished (Fig. 4). Near-bed vertical flow was on average directed downwards, and reduced towards increasing shell content (Fig. 5b). Interestingly, while the increasing near-bed flow velocity with increasing shell percentages indicates a reduction in overall bed friction (Fig. 5a), the highest TKE is observed at 50 % shell content (Fig. 5c). Overall, there is also a consistent pattern in the turbulent structure maintained between each run (Fig. S4).



285

Figure 5: Time-averaged near-bed velocity profiles showing the (a) x and (b) z direction of the constant flow experimental runs, as well as the (c) peak TKE values plotted against shell content. Note: The profiles are time-averaged, as indicated by the overbars, over the entire duration of each experimental run.

290

The critical near-bed velocity profiles from the ACC flow experimental runs showed a large reduction in critical near-bed velocity between 0 and 15 % shell content, followed by a minor reduction towards the 50 % shell content (Fig. 6a). No differences were observed between the vertical velocity profiles (Fig. 6b), which averaged 0 as the ripples were absent. Shells had a strong influence on the critical TKE and BSS (Fig. 7a). The most immediate and drastic changes in the critical BSS occurred when the smallest quantity of shell was mixed into the sediment (2.5 %), where the addition of shell material initially

295 increased the critical BSS from approximately 0.2 N m⁻² at 0 % shell content to approximately 0.75 N m⁻² at 2.5 % shell content

(Fig. 7a). Subsequently, the critical BSS dropped towards 0.25 N m^{-2} at 15 % shell content ($R^2 = 0.91$, Fig. 7a). At shell concentrations above 20 %, the critical BSS slowly increased again to approximately 0.5 N m^{-2} at 50 % shell content ($R^2 = 0.50$, Fig. 7a). In contrast to the critical BSS, the critical depth-averaged velocity for incipient motion consistently reduced towards 15 % shell content ($R^2 = 0.99$, Fig. 7b), after which it stayed constant ($R^2 = 0.29$, Fig. 7b). The quadrant analysis plots show that the turbulence-induced flow is predominantly directed forwards and downwards (Fig. S5).

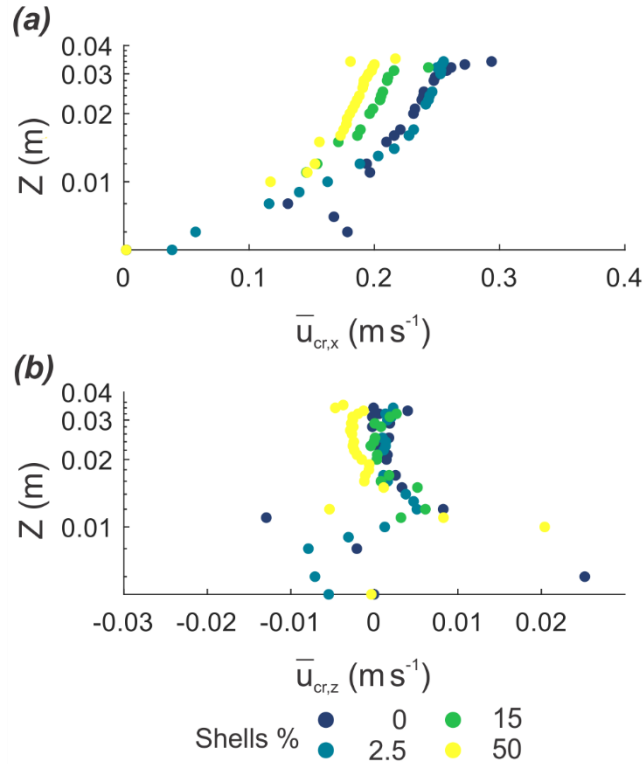


Figure 6: (a) Near-bed streamwise flow and (b) vertical flow at the onset of sediment transport for flat beds (ACC flow experiment).

Note: The overbars denote that the x-axes are time-averaged, over a 10-minute period, which encompasses the 5 minutes prior to and following the incipient motion, for the four selected experimental runs.

305

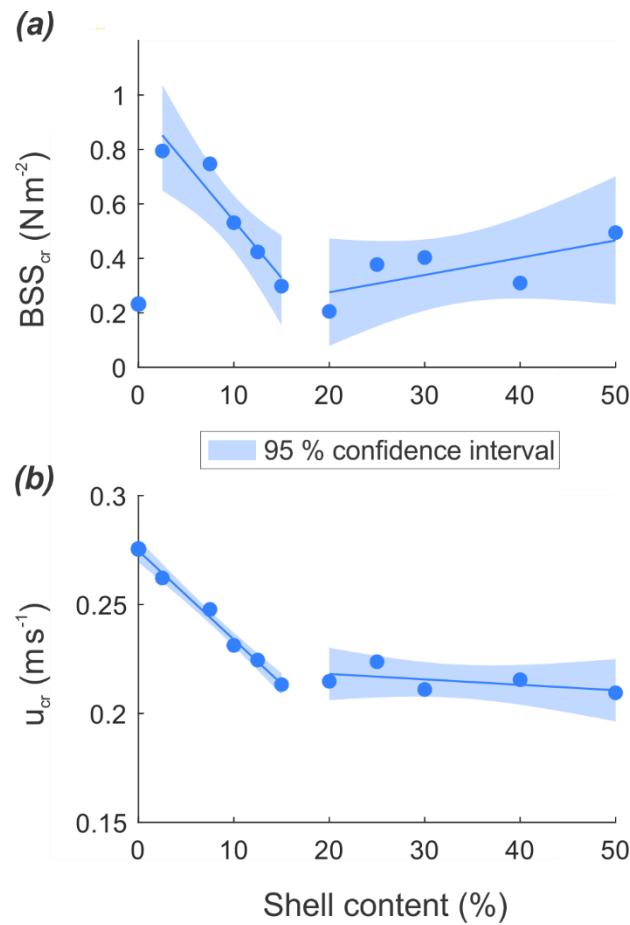


Figure 7: (a): The critical BSS for incipient motion and the (b) corresponding depth-averaged velocity for the ACC flow experiment. The shaded regions represent the 95th percentile confidence intervals.

310 The influence of shells on the total bed roughness showed contrasting behavior between flat (e.g., ACC flow
 experiment) and equilibrium (e.g., constant flow experiment) beds (Fig. 8). Under the absence of bed forms, the total bed
 roughness showed a similar trend as the critical BSS; a large increase from 1.2×10^{-4} m to 0.042 m between 0 and 7.5 % shell
 content, followed by a decrease to 0.007 m at 15 % shell content, after which it stabilized at 0.005 ± 0.004 m towards 50 %
 315 10 % shell content. Beyond 10 % shell content, the total bed roughness increased to 0.036 m.

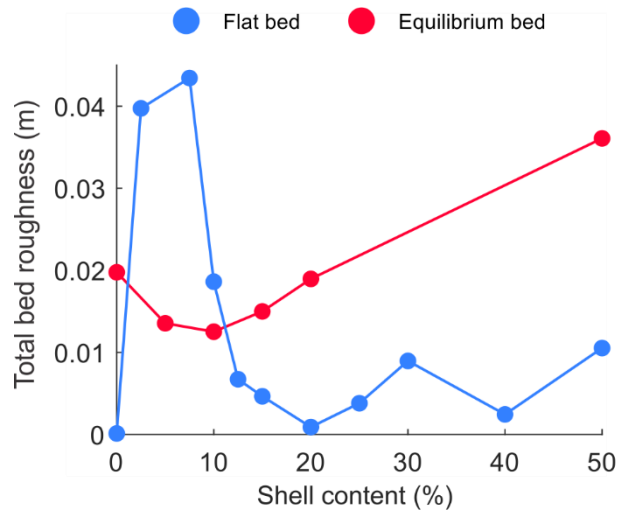


Figure 8: Total bed roughness against shell content for the flat beds (ACC flow experimental runs) and equilibrium beds (constant flow experimental runs).

4 Discussion

320

4.1 Significance of shell-ripple interactions

In gravel bed rivers, it is known that the incorporation of topography into the sediment surface creates microclusters that increase both the bed roughness as well as bed stability (Curran, 2010). The anchoring of shells, even through partial burial, in sandy sediment greatly raises their critical erosion threshold compared to individual shells situated on a flat surface, irrespective of the orientation. Whereas loose shells on top of a flat sandy surface can erode at velocities well below 40–50 cm s⁻¹ (Dey, 2003), shells that are fixed in the sediment, especially in clusters, are much less susceptible to erosion. In our experiments, the shells were almost completely immobile over the entire duration of the experimental runs, with visually no noticeable change as evidenced by both the time series photos and video footage (Fig. S2). What would appear as bands of shell is an artefact caused by the localized changes and movement of the sand, rather than a change to the shells. Despite flow velocities reaching these thresholds in our experiments, the shells were mostly immobile, even as ripples migrated over them. In rare cases, the smaller valves and fragments sometimes shifted a few centimeters due to ripple movement. But in the higher shell treatments, the shells were practically fixed structures (Fig. 3 and S2).

330

Therefore, a sandy sediment bed with sufficient quantity of shells under a unidirectional flow will produce an armoring effect somewhat similar to riverine environments, where gravel beds produce clustered structures that mediate the bed-flow interactions through a combination of bed stabilization, altered roughness and regulation of the amount of sediment available for transport (Curran, 2010; Tuijnder et al., 2009; Wilcock and Detemple, 2005). In addition, our experiments show that shell content has another indirect bed-mediating effect. Due to the dampening of the size of the ripples, and consequently

335

a reduction of the bottom roughness, there was a progressive enhancement of the mean near-bed flow (Fig. 6) as a function of increased shell content, while at the same time, a slowing down of the ripple migration rate (Fig. 4d), due to both a decrease
340 in overall sediment supply (from shell displacement) and immobile shells, even at the very low percentages.

The opposing behavior in terms of critical BSS and depth-averaged velocity indicates that shells may modify sediment-flow interactions in two ways: 1) by stabilizing the sediment, and 2) by increasing the total bed roughness and near-bed TKE. Following this, the large increase of critical BSS for low shell concentration is probably a consequence of a large increase in sediment stability or by a large increase in bed roughness, given that the reduction in critical depth-averaged
345 velocity remains minimal. In the case of low shell density, shells may disrupt flow in the boundary layer and thereby increase the TKE. For higher shell densities, flow may be deflected over the shells, which progressively reduces the disturbance of the boundary layer and thus, the TKE. Similar density-dependent alterations in flow pattern from flume studies using either live animals or mimics have also been observed (Friedrichs et al., 2000, 2009). In these studies, the erosion fluxes and deposition of suspended material were substantially enhanced when densities were such that less than 4 % of the sediment area was
350 covered, while above this coverage, both factors saw a drastic reduction.

As the flat bed transitions towards a rippled one, the initial flow and (de)stabilization effects begin to shift. As the shell content increases, the sand available for migration decreases while the immobile shells hamper ripple formation. Consequently, the attainable ripple size negatively correlates to shell content. Both the presence of ripples and shells increase the bottom roughness, and the pattern of the calculated total bed roughness, which is minimal at intermediate shell content,
355 shows both impacts. Bed roughness was actually the largest where the shell content was also highest (Fig. 8), despite the ripple size having diminished substantially. This contrasting pattern shows that, in the absence of ripples, small shell concentrations generate a high total bed roughness, but this effect is suppressed by the large ripples that are formed under these conditions at equilibrium. At high shell concentrations however, the direct effect of shells on total bed roughness is smaller, but when reinforced by the presence of small ripples, results in a higher combined net roughness (Fig. 8).

360

4.2 Potential implications of shells for larger-scale sediment dynamics

Natural sediments rarely consist of pure, clean sand, and often include other debris, fragments and particles (Earle, 2020; Gornitz, 2008; Seibold and Berger, 2017). But sediment characteristics are important for bedform development, roughness and larger-scale implications, and even minute changes can immediately impact smaller bedforms such as sand ripples. Similar
365 dampening effects have been shown for other biogenic substances and fine particles (Friend et al., 2008; van Ledden et al., 2004; Malarkey et al., 2015). Biogenic shells, given their size, density and dimensional aspects, behave very differently from sand grains (Soulsby, 1997), and, as shown here, a composition of 2.5 % shell can already drastically enhance critical BSS and total bed roughness. As the rippled bed matures, which is likely the realistic scenario in many sandy seabeds, the effects of increasing shell content becomes more evident, through patterns of bed stabilization (e.g., armoring). Our quantities of shell
370 material are well within the range observed in sandy coastal environments. At a sandy (sand wave) location within the Dutch North Sea (Cheng et al., 2020; Damveld et al., 2018), the shell content of the sediment samples was also determined. We

measured shell percentages ranging from < 1.0 to 41 % (mean = 8 %, mode = 7 %). Given the observed complexity in the near-bed flow conditions at these shell percentages, this signifies that many such sandy environments are likely to be subjected to similar sand-shell-ripple interactions.

375 The primary mechanisms driving current-generated ripple dynamics are rather well established, but good indicators are still lacking for ripple size, which is dependent on the grain size, viscosity, density and flow strength (Lapôtre et al., 2017). Most model predictions typically omit other particle types or represent the sediment by a single value (e.g., D_{50}). However, given the fact that these shell valves and fragments differ in size, shape and density from sand grains and are largely immobile in our experiments, they cannot be accurately approximated by equations developed for average sand grains. Nevertheless, the
380 addition and subsequent coarsening due to shell valves and fragments dampened the ripples up to 7-fold with height, more than 2-fold in length and with an order of magnitude reduction in migration rate (bare sand vs. 50 % shells; Fig. 4a, b and d). The effect of shells on ripple symmetry is inconclusive. There was a very slight increase in asymmetry, but this may be due more to the noise from the variability than being an actual trend (Fig. 4c).

We have shown how shell percentages around 10–15 % already reduced ripple size significantly, and above 20 %, ripples are almost entirely absent. We also observed largely-immobile clusters or bands of shells, essentially stabilizing the sediment through an armoring effect. This is perhaps most comparable with the riverine gravel-bed armoring phenomenon, where due to the coarser sediment particles and flow conditions, coarser grains are partitioned to the top. Consequently, the surface becomes a relatively immobile layer inhibiting sediment transport, among other hydrodynamic interactions (Curran, 2010; Dietrich et al., 1989; Shen and Lu, 1983; Tuijnder et al., 2009). Storm events are often necessary to cause significant
390 flushing of the lower layers or even break an armored layer (Vericat et al., 2006). It would be interesting to investigate how a large quantity of immobile shells would behave under such extreme conditions. Some evidence suggests that gravel bed armoring can persist through floods, but the level of mobility and partial replacement or renewal of grains in the surface layer is inconclusive (Wilcock and Detemple, 2005).

Care must be taken in drawing comparisons as these are dissimilar environments with entirely different causes for the
395 armoring. As mentioned above, the shells were already immobile from the start to finish in our experimental runs, and the long-term formation/evolution processes of sand-shell beds remains inconclusive. Moreover, unlike the riverine gravel, which is closer to a spherical shape, shells are an entirely separate class of materials with biological origins. Under typical unidirectional flow conditions, a higher shell % can be expected to dampen ripple development, migration and, consequently, the bedload transport. How shells might affect the hydrodynamics and bed morphology under more-complex systems and flow
400 conditions, particularly in shallower, wave-dominated environments, remains to be investigated (e.g., under sheet or oscillatory flow conditions; Nelson et al., 2013; Precht & Huettel, 2003; Soulsby, 1997).

Nevertheless, we foresee many relevant implications of shell research in geomorphologic investigations as well as coastal engineering applications. Shells clearly have the ability to regulate ripple growth and migration, and consequently the bedload transport. A good estimation on the sediment-shell composition would allow us to assess the sediment dynamics for
405 a given sandy environment and provide better insight on bed stability to produce more-accurate calculations on bedload

transport. Concurrently, given the close-coupling between sediment transport and larger-scale adaptations in seabed morphology, this information could aid in developing or utilizing better methods with regards to offshore seabed patterns, shoreline preservation, longshore sediment transport and coastal management. Our study has provided new insight on how shell material directly, and measurably, influences ripple evolution and migration in medium sand.

410

5 Conclusions

A series of sand-shell-ripple experiments were conducted to directly measure the impact of shell material on the development of current-driven ripples in sandy sediment ($D_{50} = 352 \mu\text{m}$). Our results demonstrate that the shell content has a dynamic effect on the near-bed hydrodynamics that changes over several stages. This mainly occurs as the BSS to flow velocity balance is altered, initially showing a more significant sheltering effect at low shell content ($\leq 15\%$) since higher shell quantities will disproportionately enhance the turbulence under a flat bed setting. However, when a sufficient flow velocity is achieved to generate ripples, the shell-induced turbulence will quickly be overcome by the developing bedforms and offset the initial trend. The armoring effect grows stronger with increasing shell content in the form of immobile shells.

In terms of sedimentary transport, shell compositions above 15–20% exhibit a drastic change in the ability of ripples to develop and migrate. The threshold is somewhat higher in the constant flow than in the ACC flow experiment (20% vs. 15% shells), given the much longer exposure to higher velocity and equilibrium conditions. A sandy mixture with 2.5–50% shell content increasingly dampens the ripples, thereby reducing the ripple migration by up to one order of magnitude. Moreover, these percentages are representative of certain areas within the natural environment. Thus, the presence of shells needs to be taken into account to better understand and predict the sedimentary processes, as compared to the more simplistic conditions that could be expected from purely siliciclastic sediment. Our experiments shed some light on the direct influences of shells on ripple dynamics in sandy sediment under unidirectional current-flow conditions. This work would greatly benefit from further studies utilizing other grain sizes combined with shells, as well as an investigation on the other particles of different origin, size, shape and density, but which are nevertheless also commonly found throughout the marine environment.

430 **Supplementary Materials:** Fig. S1; Fig. S2; Fig. S3; Fig. S4; Fig. S5; Table S1; Table S2; Table S3

CRediT authorship contribution statement

Chiu H. Cheng: Conceptualization, Methodology, Investigation, Formal analysis, Data Curation, Visualization, Writing – Original Draft, Writing – Review & Editing, Project administration. **Jaco. C. de Smit:** Conceptualization, Methodology, Investigation, Formal analysis, Software, Visualization, Writing – Original Draft, Writing – Review & Editing. **Greg. S. Fivash:** Methodology, Formal analysis, Software, Visualization, Writing – Original Draft, Writing – Review & Editing. **Suzanne J. M. H. Hulscher:** Writing – Review & Editing, Funding acquisition. **Bas W. Borsje:** Conceptualization, Writing – Review & Editing, Supervision. **Karline Soetaert:** Conceptualization, Writing – Review & Editing, Supervision, Resources, Funding acquisition.

Data availability. The data collected and used for this publication will be uploaded to the 4TU.ResearchData repository at the following link: (10.4121/12852113), hosted by TU Delft, The Netherlands.

Competing interests. The author declares that there is no conflict of interest.

Acknowledgements. We would like to thank Tjeerd Bouma in the planning and conceptualization of the experiment. Many thanks also to Lennart van IJzerloo, Bert Sinke and Arne den Toonder for their assistance with the setting up of the flume.

Financial support. This work is part of the NWO-ALW funded SANDBOX project. The Royal Boskalis Westminster N.V. and the Royal Netherlands Institute for Sea Research (NIOZ) are also acknowledged for their financial support of this project.

References

- Ahmerkamp, S., Winter, C., Janssen, F., Kuypers, M. M. M. and Holtappels, M.: The impact of bedform migration on benthic oxygen fluxes, *J. Geophys. Res. Biogeosciences*, 120(11), 2229–2242, doi:10.1002/2015JG003106, 2015.
- Al-Dabbas, M. A. M. and McManus, J.: Shell fragments as indicators of bed sediment transport in the Tay Estuary, *Proc. R. Soc. Edinburgh. Sect. B. Biol. Sci.*, 92(3–4), 335–344, doi:10.1017/S0269727000004759, 1987.
- Ashley, G., Boothroyd, J. C., Bridge, J. S., Clifton, H. E., Dalrymple, R., Elliott, T., Flemming, B., Harms, J. C., Harris, P., Hunter, R. E., Kreisa, R. D., Lancaster, N., Middleton, G. V, Paola, C., Rubin, D. M., Smith, J. D., Southard, J. B., Terwindt, J. H. I. and Twitchell, D. C.: Classification of large-scale subaqueous bedforms: a new look at an old problem., *J. Sediment. Petrol.*, 60, 160–172, 1990.
- 460 Baas, J. H. and De Koning, H.: Washed-out ripples; their equilibrium dimensions, migration rate, and relation to suspended-sediment concentration in very fine sand, *J. Sediment. Res.*, 65(2a), 431–435, doi:10.1306/D42680E5-2B26-11D7-8648000102C1865D, 1995.
- Baas, J. H., van Dam, R. L. and Storms, J. E. A.: Duration of deposition from decelerating high-density turbidity currents, *Sediment. Geol.*, 136(1), 71–88, doi:https://doi.org/10.1016/S0037-0738(00)00088-9, 2000.
- 465 Bartholdy, J., Ernstsens, V. B., Flemming, B. W., Winter, C., Bartholomä, A. and Kroon, A.: On the formation of current ripples, *Sci. Rep.*, 5(1), 11390, doi:10.1038/srep11390, 2015.
- Blanchard, G. F., Guarini, J.-M., Gros, P. and Richard, P.: Seasonal effect on the relationship between the photosynthetic capacity of intertidal microphytobenthos and temperature, *J. Phycol.*, 33(5), 723–728, doi:10.1111/j.0022-3646.1997.00723.x, 1997.

- 470 Borchers, H. W.: *pracma: Practical Numerical Math Functions*, [online] Available from: <https://cran.r-project.org/web/packages/pracma/index.html>, 2019.
- Brakenhoff, L., Schrijvershof, R., van der Werf, J., Grasmeyer, B., Ruessink, G. and van der Vegt, M.: From Ripples to Large-Scale Sand Transport: The Effects of Bedform-Related Roughness on Hydrodynamics and Sediment Transport Patterns in Delft3D, *J. Mar. Sci. Eng.*, 8(11), 25, 2020.
- 475 Cheng, C. H., Soetaert, K. and Borsje, B. W.: Sediment Characteristics over Asymmetrical Tidal Sand Waves in the Dutch North Sea, *J. Mar. Sci. Eng.*, 8(409), 1–16, doi:10.3390/jmse8060409, 2020.
- Curran, J. C.: An investigation of bed armoring process and the formation of microclusters, in 2nd Joint Federal Interagency Conference, pp. 1–12, Las Vegas., 2010.
- Damveld, J. H., Reijden, K. J., Cheng, C., Koop, L., Haaksma, L. R., Walsh, C. A. J., Soetaert, K., Borsje, B. W., Govers, L.
480 L., Roos, P. C., Olf, H. and Hulscher, S. J. M. H.: Video transects reveal that tidal sand waves affect the spatial distribution of benthic organisms and sand ripples, *Geophys. Res. Lett.*, 0(ja), doi:10.1029/2018GL079858, 2018.
- Damveld, J. H., Roos, P. C., Borsje, B. W. and Hulscher, S. J. M. H.: Modelling the two-way coupling of tidal sand waves and benthic organisms: A linear stability approach, *Environ. Fluid Mech.*, doi:10.1007/s10652-019-09673-1, 2019.
- Dey, S.: Incipient Motion of Bivalve Shells on Sand Beds under Flowing Water, *J. Eng. Mech.*, 129(2), 232–240,
485 doi:10.1061/(ASCE)0733-9399(2003)129:2(232), 2003.
- Dietrich, W., Kirchner, J., Ikeda, H. and Iseya, F.: Sediment Supply and Development of Coarse Surface Layer in Gravel Bedded Rivers, *Nature*, 340, doi:10.1038/340215a0, 1989.
- Earle, S.: *Sea-Floor Sediments*, [online] Available from: <https://geo.libretexts.org/@go/page/7876>, 2020.
- Friedrichs, M., Graf, G. and Springer, B.: Skimming flow induced over a simulated polychaete tube lawn at low population
490 densities, *Mar. Ecol. Prog. Ser.*, 192, 219–228, doi:10.3354/meps192219, 2000.
- Friedrichs, M., Leipe, T., Peine, F. and Graf, G.: Impact of macrozoobenthic structures on near-bed sediment fluxes, *J. Mar. Syst.*, 75(3), 336–347, doi:https://doi.org/10.1016/j.jmarsys.2006.12.006, 2009.
- Friend, P. L., Lucas, C. H., Holligan, P. M. and Collins, M. B.: Microalgal mediation of ripple mobility, *Geobiology*, 6(1), 70–82, doi:10.1111/j.1472-4669.2007.00108.x, 2008.
- 495 Gornitz, V.: *Encyclopedia of Paleoclimatology and Ancient Environments.*, 2008.
- Gutiérrez, J., Jones, C., Strayer, D. and Iribarne, O.: Mollusks as ecosystem engineers: The role of shell production in aquatic habitats, *Oikos*, 101, 79–90, doi:10.1034/j.1600-0706.2003.12322.x, 2003.
- Herman, P., Middelburg, J. and Heip, C.: Benthic community structure and sediment processes on an intertidal flat: Results

- from the ECOFLAT project, *Cont. Shelf Res.*, 21, 2055–2071, doi:10.1016/S0278-4343(01)00042-5, 2001.
- 500 Huettel, M. and Rusch, A.: Transport and degradation of phytoplankton in permeable sediment, *Limnol. Oceanogr.*, 45(3), 534–549, doi:10.4319/lo.2000.45.3.0534, 2000.
- Idier, D., Astruc, D. and Hulscher, S. J. M. H.: Influence of bed roughness on dune and megaripple generation, *Geophys. Res. Lett.*, 31(13), n/a--n/a, doi:10.1029/2004GL019969, 2004.
- Kidwell, S. M.: Palaeobiological and sedimentological implications of fossil concentrations, *Nature*, 318(6045), 457–460, 505 doi:10.1038/318457a0, 1985.
- Kösters, F. and Winter, C.: Exploring German Bight coastal morphodynamics based on modelled bed shear stress, *Geo-Marine Lett.*, 34(1), 21–36, doi:10.1007/s00367-013-0346-y, 2014.
- Langlois, V. and Valance, A.: Initiation and evolution of current ripples on a flat sand bed under turbulent water flow, *Eur. Phys. J. E*, 22(3), 201–208, doi:10.1140/epje/e2007-00023-0, 2007.
- 510 Lapôtre, M., Lamb, M. and McElroy, B.: What sets the size of current ripples?, *Geology*, 45, G38598.1, doi:10.1130/G38598.1, 2017.
- Lichtman, I. D., Baas, J. H., Amoudry, L. O., Thorne, P. D., Malarkey, J., Hope, J. A., Peakall, J., Paterson, D. M., Bass, S. J., Cooke, R. D., Manning, A. J., Davies, A. G., Parsons, D. R. and Ye, L.: Bedform migration in a mixed sand and cohesive clay intertidal environment and implications for bed material transport predictions, *Geomorphology*, 315, 17–32, 515 doi:<https://doi.org/10.1016/j.geomorph.2018.04.016>, 2018.
- Ligges, U., Short, T., Kienzle, P., Schnackenberg, S., Billinghamurst, D., Borchers, H.-W., Carezia, A., Dupuis, P., Eaton, J. W., Farhi, E., Habel, K., Hornik, K., Krey, S., Lash, B., Leisch, F., Mersmann, O., Neis, P., Ruohio, J., Smith, J. O., Stewart, D. and Weingessel, A.: signal: Signal Processing, [online] Available from: <https://cran.r-project.org/web/packages/signal/index.html>, 2015.
- 520 Malarkey, J., Baas, J. H., Hope, J. A., Aspden, R. J., Parsons, D. R., Peakall, J., Paterson, D. M., Schindler, R. J., Ye, L., Lichtman, I. D., Bass, S. J., Davies, A. G., Manning, A. J. and Thorne, P. D.: The pervasive role of biological cohesion in bedform development, *Nat. Commun.*, 6, 6257, doi:10.1038/ncomms7257, 2015.
- Miedema, S. and Ramsdell, R.: Hydraulic transport of sand/shell mixtures in relation with the critical velocity, *Terra Aqua*, 122, 2011.
- 525 Mietta, F., Chassagne, C., Manning, A. J. and Winterwerp, J. C.: Influence of shear rate, organic matter content, pH and salinity on mud flocculation, *Ocean Dyn.*, 59(5), 751–763, doi:10.1007/s10236-009-0231-4, 2009.
- Nelson, T. R., Voulgaris, G. and Traykovski, P.: Predicting wave-induced ripple equilibrium geometry, *J. Geophys. Res. Ocean.*, 118(6), 3202–3220, doi:<https://doi.org/10.1002/jgrc.20241>, 2013.

- Nowell, A. R. M. and Jumars, P. A.: Flow Environments of Aquatic Benthos, *Annu. Rev. Ecol. Syst.*, 15(1), 303–328, doi:10.1146/annurev.es.15.110184.001511, 1984.
- 530 Paterson, A., Hume, T. and Healy, T.: River Mouth Morphodynamics on a Mixed Sand-Gravel Coast, *J. Coast. Res.*, 288–294 [online] Available from: <http://www.jstor.org/stable/25736295>, 2001.
- Pilditch, C. A., Emerson, C. W. and Grant, J.: Effect of scallop shells and sediment grain size on phytoplankton flux to the bed, *Cont. Shelf Res.*, 17(15), 1869–1885, doi:[https://doi.org/10.1016/S0278-4343\(97\)00050-2](https://doi.org/10.1016/S0278-4343(97)00050-2), 1997.
- 535 Pope, N., Widdows, J. and Brinsley, M.: Estimation of bed shear stress using the turbulent kinetic energy approach—A comparison of annular flume and field data, *Cont. Shelf Res.*, 26, 959–970, doi:10.1016/j.csr.2006.02.010, 2006.
- Precht, E. and Huettel, M.: Advective pore-water exchange driven by surface gravity waves and its ecological implications, *Limnol. Oceanogr.*, 48(4), 1674–1684, doi:10.4319/lo.2003.48.4.1674, 2003.
- Ramsdell, R. and Miedema, S.: Hydraulic transport of sand/shell mixtures, in *WODCON XIX*, pp. 1–21, Beijing., 2010.
- 540 Russell-Hunter, W. D.: Overview: Planetary Distribution of and Ecological Constraints upon the Mollusca, *Ecology*, 1–27, 1983.
- Seibold, E. and Berger, W.: Sources and Composition of Marine Sediments BT - *The Sea Floor: An Introduction to Marine Geology*, edited by E. Seibold and W. Berger, pp. 45–61, Springer International Publishing, Cham., 2017.
- Shen, H. W. and Lu, J.: Development and Prediction of Bed Armoring, *J. Hydraul. Eng.*, 109(4), 611–629, doi:10.1061/(ASCE)0733-9429(1983)109:4(611), 1983.
- 545 Soulsby, R.: Chapter 5 The Bottom Boundary Layer of Shelf Seas, in *Physical Oceanography of Coastal and Shelf Seas*, vol. 35, edited by B. B. T.-E. O. S. Johns, pp. 189–266, Elsevier., 1983.
- Soulsby, R.: *Dynamics of Marine Sands: A manual for Practical Applications*, Thomas Telford Publishing., 1997.
- Sugiyama, J. and Kobayashi, K.: wvtool: Image Tools for Automated Wood Identification, [online] Available from: <https://cran.r-project.org/web/packages/wvtool/index.html>, 2016.
- 550 Tuijnder, A. P., Ribberink, J. A. N. S. and Hulscher, S. J. M. H.: An experimental study into the geometry of supply-limited dunes, *Sedimentology*, 56(6), 1713–1727, doi:<https://doi.org/10.1111/j.1365-3091.2009.01054.x>, 2009.
- van Ledden, M., van Kesteren, W. G. M. and Winterwerp, J. C.: A conceptual framework for the erosion behaviour of sand–mud mixtures, *Cont. Shelf Res.*, 24(1), 1–11, doi:<https://doi.org/10.1016/j.csr.2003.09.002>, 2004.
- 555 Van Oyen, T., de Swart, H. E. and Blondeaux, P.: Bottom topography and roughness variations as triggering mechanisms to the formation of sorted bedforms, *Geophys. Res. Lett.*, 37(18), 1–5, doi:10.1029/2010GL043793, 2010.
- van Rijn, L. C., Nieuwjaar, M. W. C., van der Kaay, T., Nap, E. and van Kampen, A.: Transport of Fine Sands by Currents

- and Waves, *J. Waterw. Port, Coastal, Ocean Eng.*, 119(2), 123–143, doi:10.1061/(ASCE)0733-950X(1993)119:2(123), 1993.
- 560 van Rijn, L. C.: *Principles of Sediment Transport in Rivers, Estuaries and Coastal Seas*, Aqua Publications. [online] Available from: <https://books.google.nl/books?id=gGIYAQAAlAAJ>, 1993.
- Vericat, D., Batalla, R. J. and Garcia, C.: Breakup and reestablishment of the armour layer in a large gravel-bed river below dams: The lower Ebro, *Geomorphology*, 76(1), 122–136, doi:<https://doi.org/10.1016/j.geomorph.2005.10.005>, 2006.
- Wilcock, P. and Detemple, B.: Persistence of Armor Layers in Gravel-Bed Streams, *Geophys. Res. Lett.*, 32, doi:10.1029/2004GL021772, 2005.
- 565 Witbaard, R., Bergman, M. J. N., van Weerlee, E. and Duineveld, G. C. A.: An estimation of the effects of *Ensis directus* on the transport and burial of silt in the near-shore Dutch coastal zone of the North Sea, *J. Sea Res.*, 127, 95–104, doi:10.1016/j.seares.2016.12.001, 2016.